CHEMISTRY OF MATERIALS
Cite This: Chem. Mater. 2017, 29, 10518−10525
Article
pubs.acs.org/cm

Formation of Au Nanoparticles in Liquid Cell Transmission Electron Microscopy: From a Systematic Study to Engineered Nanostructures

Yucheng Zhang,* Debora Keller, Marta D. Rossell, and Rolf Erni*

Electron Microscopy Center, Empa, Swiss Federal Laboratories for Materials Science and Technology, Überlandstrasse 129, CH-8600 Dübendorf, Switzerland

Supporting Information

ABSTRACT: In this work, a systematic study of the effect of electron dose rate, solute concentration, imaging mode (broad beam vs scanning probe mode), and liquid cell setup (static vs flow mode) on the growth mechanism and the ultimate morphology of Au nanoparticles (NPs) was performed in chloroauric acid ($HAuCl_4$) aqueous solutions using in situ liquid-cell TEM (LC-TEM). It was found that a diffusion limited growth dominates at high dose rates, especially for the solution with the lowest concentration (1 mM), resulting in formation of dendritic NPs. Growth of 2D Au plates driven by a reaction limited mechanism was only observed at low dose rates for the 1 mM solution. For the 5 mM and 20 mM solutions, reaction limited growth can still be induced at higher dose rates, due to abundance of the precursor available in the solutions, leading to formation of 2D plates or 3D faceted NPs. As a proof-of-concept, an Au nanostructure with a 3D faceted particle core and a dendritic shell can be in situ produced by simply tuning the electron dose in the 1 mM solution irradiated in a flow cell setup in the STEM mode. This work paves the way to study the growth of complex heteronanostructures composed of multiple elements in LC-TEM.

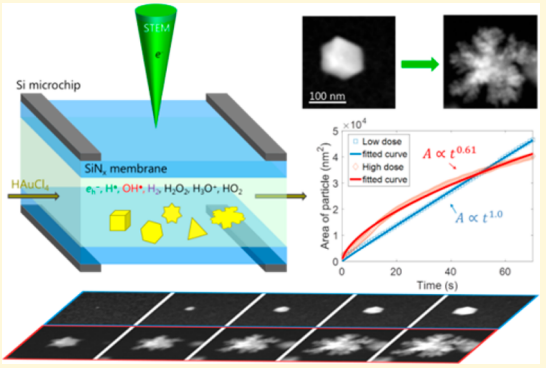

1. INTRODUCTION

In situ liquid cell transmission electron microscopy (LC-TEM) allows direct observations of dynamic processes of specimens immersed in liquids.[1,2] With its unprecedented spatial and temporal resolution, LC-TEM opens new possibilities for a wide range of research topics including nanoparticle (NP) synthesis,[3−5] nanostructure self-assembly,[6,7] and electrochemical processes in batteries[8,9] as well as life science.[10,11] Among these, studies of NP synthesis using LC-TEM have provided important insights into the underlying mechanisms in nucleation and growth, which enables design and fabrication of functional NPs with unique properties by precisely controlling their size, shape, and composition. For instance, in Zheng et al.'s pioneering work LC-TEM was adopted to directly observe the nucleation and coalescence of Pt NPs in solution, unravelling two different growth pathways, which are monomer addition and particle coalescence.[3] Similarly, in Nielsen et al.'s work, nucleation of $CaCO_3$ was observed in LC-TEM, indicating that multiple nucleation pathways are simultaneously operative.[12] These in situ studies have thus challenged the classical nucleation theory (CNT) and demand for a new examination of the mechanisms that control the nucleation and growth of nanoparticles, in order to achieve NPs and nanostructures with defined size, shape, and composition. Indeed, research in this field has been thriving due to the advancement in LC-TEM.

Although tremendous research interest has been aroused in LC-TEM and rapid progress has been achieved, there still remain challenges and difficulties to fully exploit the technique. One main challenge is to understand the complex interaction between the high energy electron and the liquid, which creates a rich amount of radicals that can significantly modify the characteristics of the specimen to be investigated. On the other hand, controlled irradiation of liquids with electrons can be exploited to induce nucleation and growth of NPs with targeted morphology, enabling direct observation of the dynamic processes. Consequently, several studies have focused on understanding these complex interactions. For instance, using a mathematical model Schneider et al. have calculated the concentrations of various radical groups and molecules created in water by the high energy electrons and their evolution with time.[13] The model helped to interpret qualitatively phenomena observed in LC-TEM, such as growth, stabilization, or etching of Au NPs depending on the electron-induced variation of the solution chemistry. Abellan et al. have studied the effect of electrons in various solvents, in order to produce net reducing or oxidizing conditions in the solution and hence gain control over growth of NPs.[14,15] Although these works have already shed light on important aspects, the findings were always

Received: October 20, 2017
Revised: November 24, 2017
Published: November 27, 2017

DOI: 10.1021/acs.chemmater.7b04421
Chem. Mater. 2017, 29, 10518−10525

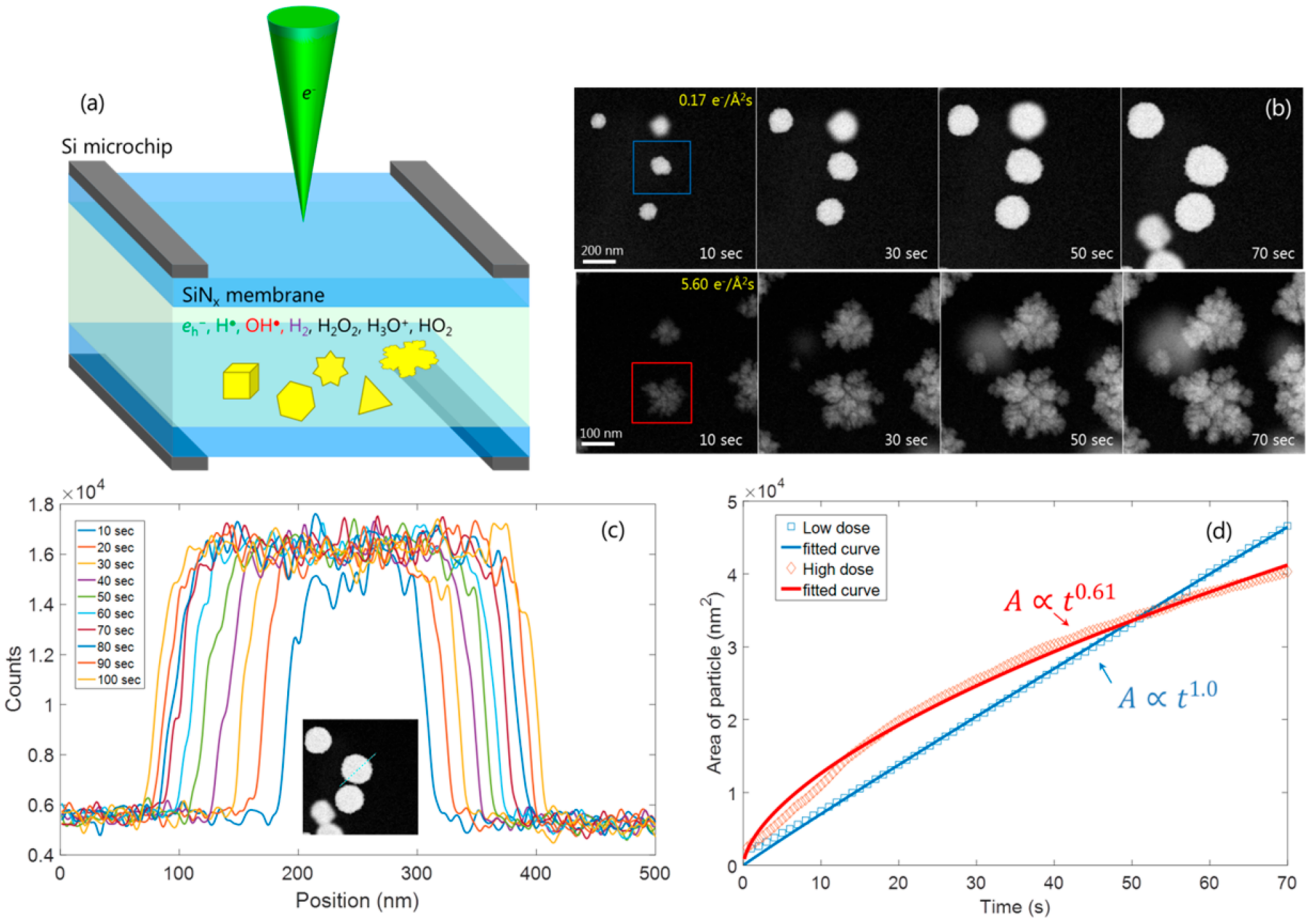

Figure 1. (a) Schematic illustration of the setup for the LC-TEM experiments. (b) Time-series of HAADF-STEM images showing the growth of Au nanoparticles in a 1 mM $HAuCl_4$ solution induced by the electron beam at two dose rates: the upper row at a low dose rate of 0.17 $e^-/(Å^2\ s)$ and the lower row at a high dose rate of 5.60 $e^-/(Å^2\ s)$. (c) Line profiles of the image intensity for the selected particle (in the inset) grown at the low dose. (d) Measured area of the particle increasing with time from the time series. The data was fitted with a power law model. The selected particles are denoted by the boxes in (b).

implemented on a specific condition in terms of solution concentration, microscopy mode (dose rates, acceleration voltage, TEM or scanning TEM (STEM)), and liquid system (cell geometry, static or flowing loading of solution). Thus, it is in general difficult to compare and combine different studies to acquire an overall picture.

In this work, growth of Au NPs induced by electron irradiation in $HAuCl_4$ aqueous solutions was systematically studied using LC-TEM. The formation of the NPs was due to the reducing effect of hydrated electrons produced by the primary electron beam in the solution. In particular, the effect of the electron dose rate and the solution concentration on the growth mechanism was quantitatively characterized, thus providing important insights into the complex interactions between the electrons and the liquids. The influence of the imaging mode used, i.e., TEM vs STEM, and the liquid cell setup, i.e., static and flow, were also compared and discussed. In this way, controlled growth of Au NPs was rationally designed and exemplified by the formation of a nanostructure composed of a 3D faceted particle core and a dendritic shell in LC-TEM.

2. EXPERIMENTS

Liquid Cell Preparation. High purity $HAuCl_4{\cdot}3H_2O$ powder (>99.9%) and deionized water were purchased from Sigma-Aldrich. Solutions of 1 mM, 5 mM, and 20 mM were prepared by adding 2 mg, 10 mg, and 40 mg of $HAuCl_4{\cdot}3H_2O$ powder into 5 mL of H_2O. A Protochips Poseidon Select holder compatible with a Thermo-Fisher Scientific Titan Themis microscope was used for the experiments. The liquid cell was assembled with a pair of small and large Si chips with a 50 × 500 μm^2 SiN_x window of a thickness of 50 nm. A 150 nm gold spacer, for both static and flow setups, is present between the chips and thus defines the minimum thickness of the liquid studied in LC-TEM. Before loading the solution, the chips were treated with O_2 plasma to improve hydrophilicity of the SiNx windows. A volume of 0.5 μL of the solution was then cast on the window and studied in the static cell setup. For the flow cell setup, the solution was continuously injected into the cell through a PEEK inlet tube with a syringe pump while TEM induced growth and imaging were operated simultaneously. Typically, a flow rate of 50 μL/h was employed during the TEM observation.

LC-TEM Experiments. The cells containing the $HAuCl_4$ solution were studied with TEM and STEM imaging using a Titan Themis microscope operated at 300 kV. High angle annular dark field in the STEM mode (HAADF-STEM), which provides high contrast from Au nanoparticles, was routinely used. The dose rate was controlled by changing gun lens, condenser lenses, probe illumination, and magnification. Time series were recorded with a typical frame time of 2−4 frames/s and 200−500 frames/series. Time series in the TEM modes was recorded using a FEI CETA 2 camera with a typical image resolution of 1024 × 1024 $pixel^2$ (binning by 4 to enhance the signal-to-noise ratio) and 40 frames/s. The TEM dose rates were calculated by dividing the beam current measured from the phosphor screen by the illumination area. To minimize the bowing effect of the SiNx

DOI: 10.1021/acs.chemmater.7b04421
Chem. Mater. 2017, 29, 10518−10525

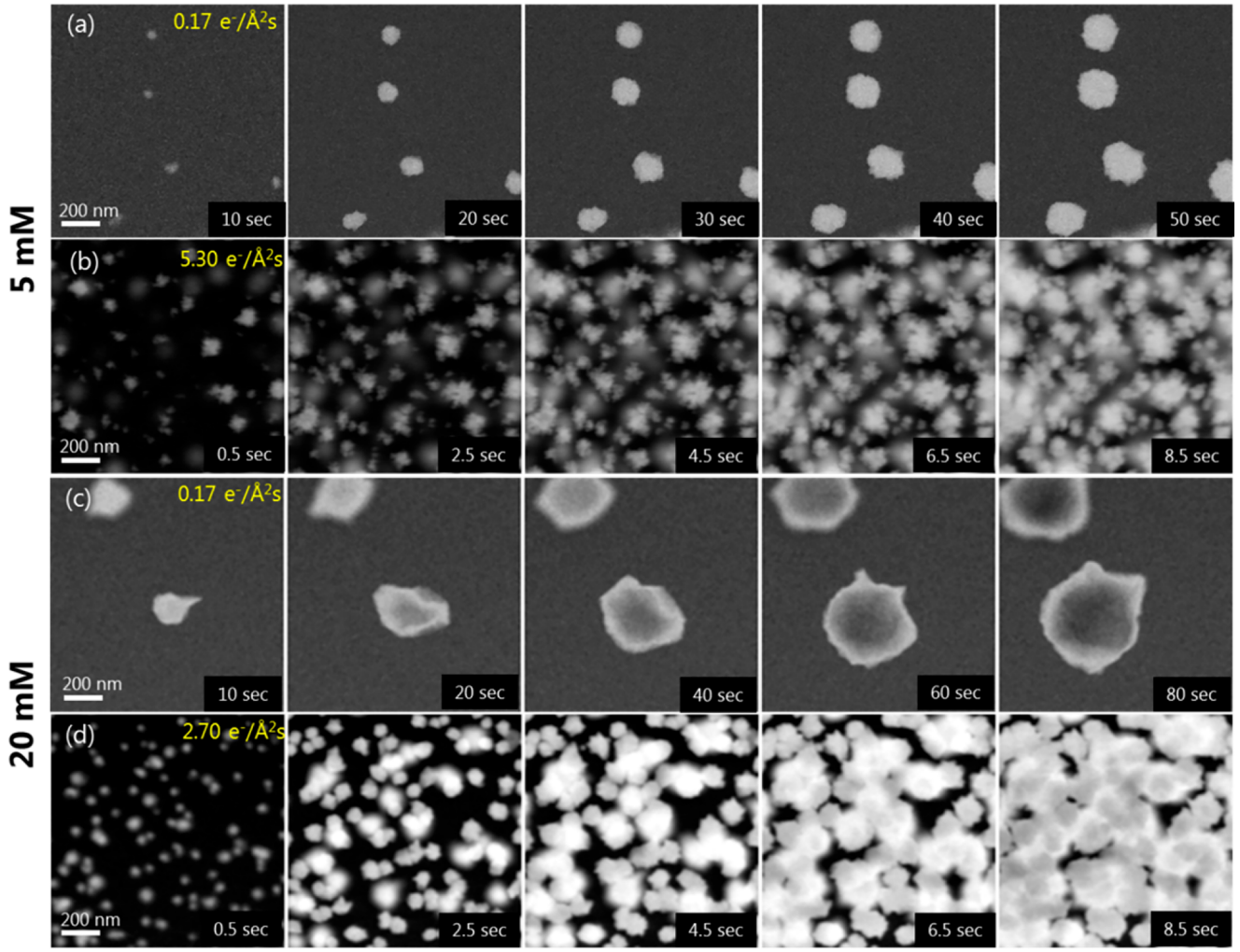

Figure 2. Time series of HAADF-STEM images showing the different morphologies of Au NPs (a, b) in a 5 mM solution induced by low (0.17 $e^-/(Å^2\ s)$) and high (5.30 $e^-/(Å^2\ s)$) electron dose rates; (c, d) in a 20 mM $HAuCl_4$ solution induced by low (0.17 $e^-/(Å^2\ s)$) and high (2.70 $e^-/(Å^2\ s)$) electron dose rates.

windows, imaging was mainly performed near the edges where the thickness of the liquid layer was smallest.

Data Processing. The time series recorded in TEM and STEM were processed using ImageJ and DigitalMicrograph. The series were normally filtered with a 3D Gaussian filter ($2 \times 2 \times 2$) and rebinned by four frames to improve the signal-to-noise ratio. To measure the particle size and the growth rate, the processed images were first segmented by automatically selecting a threshold value for the intensity using the MaxEntropy algorithm in ImageJ. The segmented binary images were then used for measuring the number of particles, n, and the area A of each particle. An effective radius r_{eff} of the particle was defined by $\sqrt{(A/\pi)}$. The growth rate curves were fitted with a power law relationship in Matlab.

3. RESULTS AND DISCUSSION

3.1. Effect of Dose Rate. The setup for the LC-TEM experiments is schematically shown in Figure 1a. A solution of 1 mM $HAuCl_4$ was first sealed hermetically between two Si microchips with thin SiNx windows. Using STEM, an electron probe of about 1 Å in diameter was scanned across the window region, inducing the growth of Au NPs while simultaneously imaging the growth dynamics. When the high energy electrons are injected into the solution, reactive radicals and molecules including e_h^-, $H^\bullet$, $OH^\bullet$, H_2, H_2O, and H_3O^+, and $HO_2^\bullet$ are produced through radiolysis reactions. The hydrated electron e_h^- is highly reducing and hence responsible for the reduction of Au^{3+} ions into Au atoms, inducing the nucleation and growth of the Au NPs. The morphologies of the NPs are closely related to the growth mechanisms, which were found to be tunable by the electron dose rate. As shown in Figure 1b, at a low dose rate of 0.20 $e^-/(Å^2\ s)$ seemingly spherical particles were formed, while at a high dose rate of 5.60 $e^-/(Å^2\ s)$ the morphology was radically different, exhibiting irregular dendritic nanostructures. Videos S1_a and S2_a in the Supporting Information are the movies recording the growth. Based on the time series of HAADF-STEM images, the characteristics of the growth can be qualitatively and quantitatively revealed. The spherical particles produced at the low dose rate appear to possess a 2D plate structure, as indicated by the time-evolved intensity profiles measured across the particle (Figure 1c). The HAADF-STEM images have a contrast proportional to the atomic number and the thickness of the particle in the beam direction. As shown in Figure 1c, the contrast increased from 10 to 20 s and then remained constant until the end of the time series, indicating the unchanged thickness of the plates. A similar observation was previously reported by Alloyeau et al.[16] The formation of plate nanostructures was attributed to a reaction limited growth driven by thermodynamic rather than kinetic effects. Indeed, by

DOI: 10.1021/acs.chemmater.7b04421
Chem. Mater. 2017, 29, 10518−10525

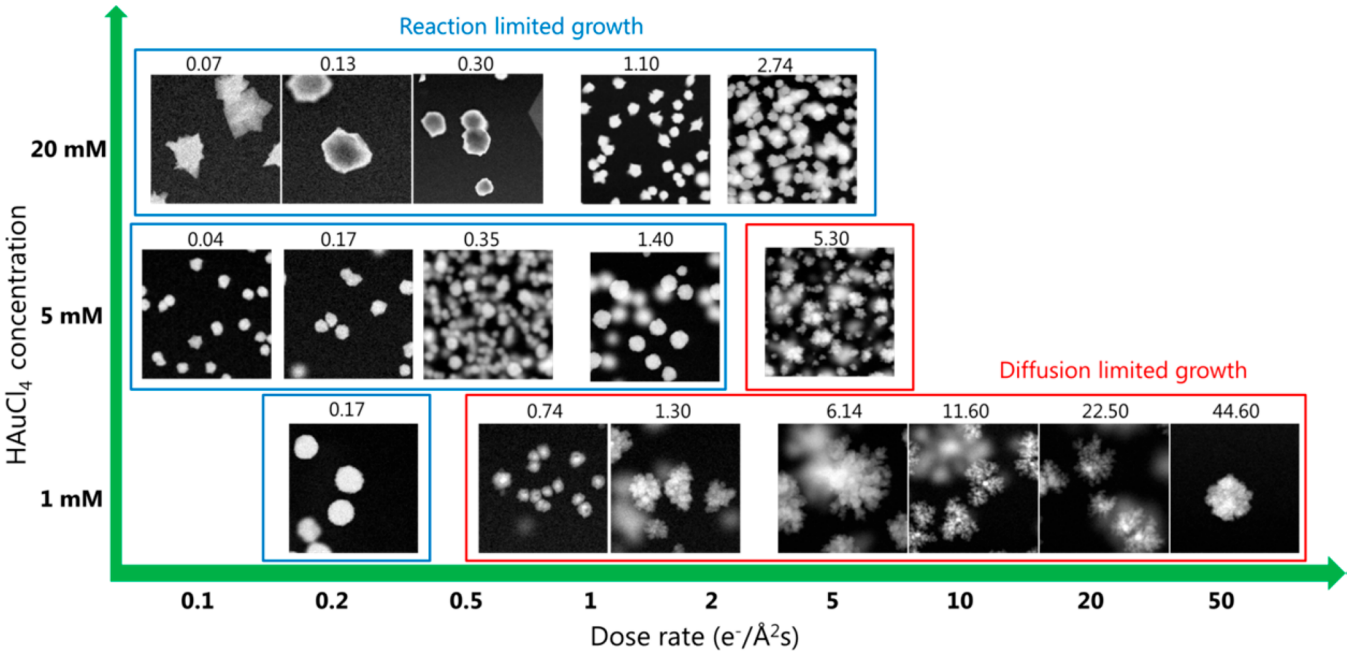

Figure 3. Effect of the dose rate and the solute concentration on the growth mode and ultimate morphology of the Au NPs induced by the electron beam in LC-TEM. The number on each image denotes the dose rate. Images in the blue box indicate reaction limited growth with a 2D plate (1 mM and 5 mM) or 3D particle (20 mM) morphology, and those in the red box indicate diffusion limited growth with a dendritic morphology.

measuring the growth rate the reaction limited growth mechanism, as defined by the Lifshitz–Slyozov–Wagner (LSW) model,[17,18] can be quantitatively confirmed. The projected areas of the particles that evolved with time are plotted in Figure 1d and were fitted with a power law model as $A = \alpha t^{\beta}$ and subsequently the effective radius $r_{eff} \propto t^{n}$ where $n = \beta/2$. The validity of the measurement of the projected area using automatically segmented images can be examined in Videos 1_b and 2_b in the Supporting Information. The curves in Figure 1d clearly showed different growth kinetics for the plate and the dendritic particles. The former features a linear curve with a constant growth rate, i.e., $\beta = 1$. For the dendritic particle, β is around 0.6, significantly less than unity. Subsequently, an effective radius $r_{eff} \propto t^{n}$ with $n = 1/2$ for the plates and approximately $n = 1/3$ for the dendrites was obtained. This is consistent with the reaction limited ($r_{eff} \propto t^{1/2}$) growth and the diffusion limited ($r_{eff} \propto t^{1/3}$) growth proposed by the LSW model. Moreover, it was found that further increasing the dose rate resulted in the similar dendritic morphology with β less than 1 (Figure S1 in the Supporting Information). Measurements from several dendritic NPs showed that a range of n values between 0.25 and 0.40 could be achieved. A previous study by Woehl et al. has shown that electron beam induced growth of Ag NPs in $AgNO_3$ solution followed diffusion limited growth with $r_{eff} \propto t^{n}$ where $n = 1/6$.[19] They attributed the significantly slower growth rate to the interaction between the particles as well as the influence from the SiN_x window, which could also explain the low n measured here. Indeed, the LSW model assumes precipitation of particles in a free solution, without considering the effect of interactions between the particles as well as the substrate. Due to the high density of Au nuclei produced at the high dose rate, the particles are adjacent to each other, which may quickly cause local depletion of precursors, hence reducing the growth rate. The nonconductive SiNx membrane can accumulate positive charges rendered by the electron beam and influence the growth in a complex way. In addition, the dendritic particles possess a 3D nanostructure. Therefore, the r_{eff} measured from the 2D projected area may have underestimated the growth rate for some particles. On the other hand, for the measured value of $1/3 < n < 1/2$, the growth was likely controlled by a mixed diffusion–reaction mechanism, where the evolution of the effective radius r_{eff} with the time t can no longer be simplified as an one-term power-law model.[18] While the dendritic Au NPs have been observed and modeled in previous works,[20,21] our analysis provides further insights in a quantitative way into the growth mechanism. All the Au plates observed in the solution followed a linear growth rate, that is, driven by a reaction limited growth with $n = 1/2$.

3.2. Effect of Solute Concentration. In addition to the 1 mM solution, 5 mM and 20 mM $HAuCl_4$ solutions were also studied using similar conditions in LC-TEM. Figure 2 presents two time series of HAADF-STEM images showing the growth of Au NPs induced in the solutions irradiated with low and high dose rates. The increasing concentration of the solutes results in a higher concentration of H^+, Cl^-, and $AuCl_3^-$ ions and a reduced pH value, modifying the kinetics in the growth and hence the morphology of the particles. In the work by Hermannsdörfer et al., it was observed that the Au NPs could dissolve, remain the same size, or grow, depending on the pH value of the solution.[22] In our experiments, all particles were observed to grow during irradiation in the static liquid-cell setup. For the 5 mM solution, growth of Au plates similar to those in the 1 mM solution was observed at a low dose rate, as shown Figure 2a. They became dendritic only when a high dose rate, i.e., more than 5 $e^-/(Å^2\ s)$, was applied (Figure 2b). For the 20 mM solution at a low dose rate, the Au NPs grew in all directions, thus forming a 3D particle with spikes (Figure 2c,d). This is evidenced by the increasingly darker contrast observed in the center of the particles as their size becomes larger. Due to the increasing dimensions of the particles, transmission of the incident electrons decreases at the center of the particles, where

DOI: 10.1021/acs.chemmater.7b04421
Chem. Mater. 2017, 29, 10518–10525

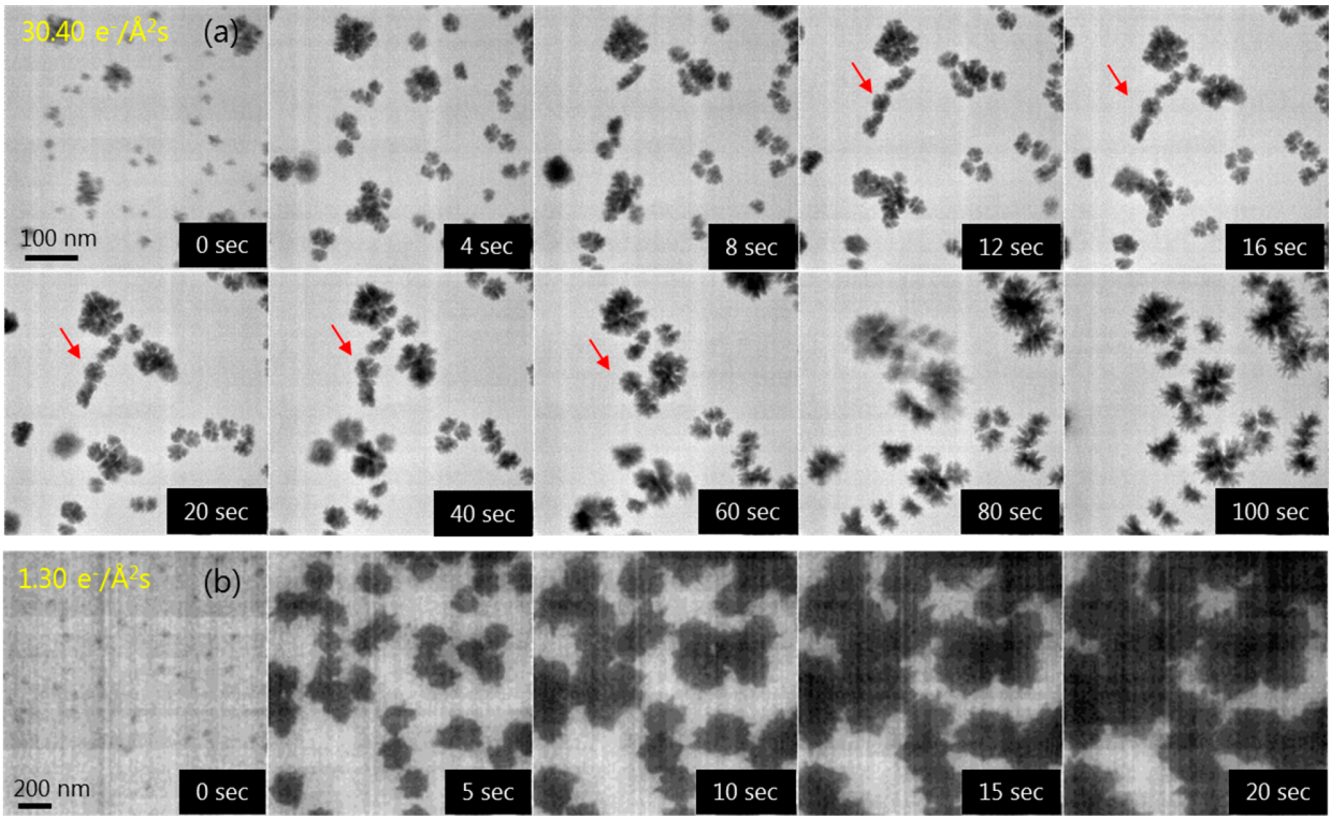

Figure 4. Time series of TEM images showing (a) growth of Au dendritic nanostructure induced with a 30.40 $e^-/(Å^2\ s)$ dose rate in a 1 mM $HAuCl_4$ solution and (b) growth of Au 3D nanoparticles with spikes induced with a 1.30 $e^-/(Å^2\ s)$ dose rate in a 20 mM $HAuCl_4$ solution. The red arrow in (a) denotes the formation and breakdown of a self-aligned chain of Au NPs.

the thickness is largest, resulting in a reduced HAADF signal. More details can be found in Figure S2 in the Supporting Information. The same morphology remained when increasing the dose rate from 0.20 to 2.70 $e^-/(Å^2\ s)$. The growth of the spikes does not become more pronounced at the higher dose rate. The morphology is attributed to the abundance of precursors in the solution. However, the growth rate was about 1 order of magnitude higher. The nucleation rate increased clearly with a higher dose rate in both solutions, due to the increasing amount of reducing agents produced and consequently a higher density of Au atoms available for nucleation.

Furthermore, by comparing all the data on the three solutions irradiated with different electron dose rates, a general trend in the effect of the dose rate and the solution chemistry on the growth mechanisms and the morphology can be obtained, as shown in Figure 3. For the low concentration solution of 1 mM, formation of Au plates was only observed at a very low dose rate, i.e., less than 0.5 $e^-/(Å^2\ s)$. Any dose rate above this value produced dendritic particles controlled by diffusion limited growth; for the intermediate concentration of 5 mM, the threshold shifted to a higher value around 5 $e^-/(Å^2\ s)$, below which the plate structure was observed; for the high concentration solution of 20 mM, only 3D particles with spikes were obtained at all the dose rates, and they all followed a linear growth rate, indicative of a reaction limited growth. At a higher dose rate of 2.0−5.0 $e^-/(Å^2\ s)$, the growth in the 20 mM solution was so fast that the irradiated area was covered entirely with Au within a few seconds. Therefore, it could be inferred that the diffusion limited growth was only possible at a dose rate much higher than 5 $e^-/(Å^2\ s)$. The observed trend can be explained by the growth kinetics in the solutions. The 1 mM solution has the fewest ion precursors $AuCl_3^-$ to react with the hydrated electrons, therefore causing the depletion of Au atoms within the irradiated region. The continuous growth of the particles requires diffusion of the ions from the outside of the region. For the 5 mM and 20 mM solutions there are abundant precursors available for the reduction reaction. Therefore, the depletion, which renders a diffusion limited growth with dendritic NPs, takes place at a higher dose rate in a higher concentration solution. However, the exact threshold value for each concentration, above which the growth mechanism changes from reaction limited toward diffusion limited, may also depend on other factors. In particular, the experiment conditions such as the electron beam energy, the imaging mode (TEM or STEM), the history of the electron dose delivery (especially for the static cell), and the chemistry of the solution that includes intentional or unintentional addition of scavengers into the solution, can all have an influence on the growth kinetics.[14,15]

3.3. TEM vs STEM. To examine the effect of the operation mode, time series of TEM images were also recorded for the 1 mM and 20 mM solutions, as shown in Figure 4. The corresponding movies are presented in Videos S3 and S4 in the Supporting Information. Au nanostructures similar to those grown in the STEM mode were also observed in TEM. For the 1 mM solution irradiated with a high dose rate of 30 $e^-/(Å^2\ s)$, particles with dendritic morphology were observed (in Figure 4a). The growth stopped after only a few seconds, followed by migration, rotation, and aggregation of the particles, indicating that the precursors were mostly depleted. With a continuous irradiation for an extended time, e.g., after about 50 s, further growth of dendrites with finer structures could be observed,

DOI: 10.1021/acs.chemmater.7b04421
Chem. Mater. 2017, 29, 10518−10525

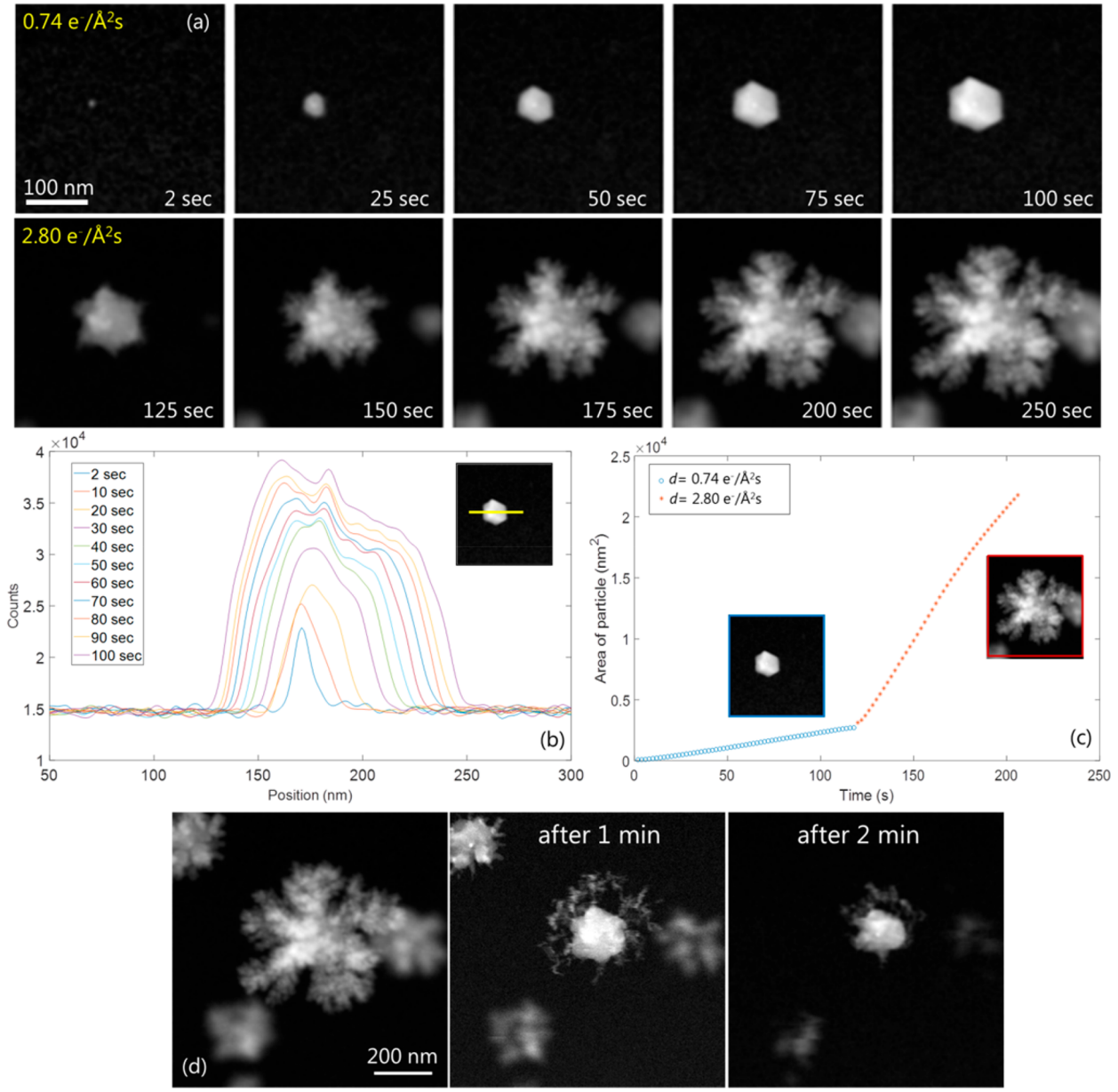

Figure 5. (a) Time series of HAADF-STEM images showing formation of an engineered Au nanostructure with a faceted particle core and a dendritic shell by simply changing the dose rate of the electron beam in a 1 mM $HAuCl_4$ solution using LC-TEM operated in a flow mode. (b) Line profiles of the image intensity across the core indicating a 3D particle. (c) The time evolution of the particle area measured from the time series. (d) HAADF-STEM images showing the etching of the Au NP by the solution in the flow mode when the electron irradiation was interrupted: the original particle (left), without electron irradiation after 1 min (middle) and after 2 min (right). Both the dendritic shell and the faceted particle core were dissolved by the solution.

which was probably due to the diffusion of the precursors from outside the field of view into the region. Similar results were also obtained for the 1 mM solution irradiated with an intermediate dose rate of 7.60 $e^-/(Å^2\ s)$, as shown in Figure S3. Dendritic growth was induced with a lower growth rate at this dose rate. Interestingly, formation of self-organized nanostructures such as a chain of Au NPs (denoted by the arrow in Figure 4a) could be observed, which was not obtainable in the STEM mode. For the 20 mM solution (in Figure 4b), the electron beam irradiation in TEM mode with a dose rate of 1.30 $e^-/(Å^2\ s)$ induced a continuous growth of 3D particles with spikes as observed in STEM. A reaction limited growth therefore prevailed with this concentration in both operation modes. In addition, the TEM mode permitted the acquisition of images at a higher temporal resolution, i.e., 40 frames/s as opposed to 2−4 frames/s in STEM.

3.4. Engineered Core−Shell Au Nanostructure. With the knowledge of the effect of the dose rate and the solution chemistry on the growth kinetics, growth of a tailored Au nanostructure can be accomplished in situ. The novel core−shell nanoparticles can be achieved by simply tuning the dose rate. As a proof of concept, a core−shell nanostructure with a faceted particle core and a dendritic shell was grown in the 1 mM $HAuCl_4$ solution, as shown in Figure 5. In order to eliminate depletion and illumination history effects, the process was performed with a flow liquid-cell setup. In this setup, a fresh solution was continuously injected into the cell during the particle growth and observation. Compared to the static cell,

DOI: 10.1021/acs.chemmater.7b04421
Chem. Mater. 2017, 29, 10518−10525

the flow setup has an impact on the equilibrium concentrations of precursors and radiolysis products which are reached under a certain electron dose. Therefore, it is expected that the threshold for the dose rate, which separates the different growth regimes, shifts accordingly, and the growth rate is altered in the presence of flow. However, the general trends for tuning the growth mode and particle morphology are expected to apply similarly in both the flow and static modes. In addition, the constant solution conditions in the flow mode ensure reproducible experimental conditions even during extended irradiation durations. Starting with a low dose rate of 0.74 $e^-/(Å^2\ s)$, the nucleation and growth of a faceted particle was initiated, as shown in Figure 5a. The intensity of the particle measured from the line profile in Figure 5b increased continuously with time, demonstrating growth of a 3D nanoparticle, which in this case was an Au cube, most likely truncated by the SiNx window, viewed in the [111] orientation. A linear growth rate of about 200 nm^2/s could be measured from the growth curve shown in Figure 5c. After growing the cube under the reaction limited condition at a low dose rate, the growth of the dendritic shell was promoted by increasing the dose rate to 2.80 $e^-/(Å^2\ s)$. The branches appeared to grow preferentially from the vertices of the cube. The ultimate morphology of the particle inherited the original symmetry of the core, and its projection resembled a nanosnowflake. To better illustrate the core−shell nature of the nanostructure, a 3D visualization using time series of the segmented HAADF images recording the growth is provided in Figure S4 in the Supporting Information. The growth rate of the shell was higher initially and gradually decreased following a diffusion limited mechanism as discussed earlier. Ahmad et al. observed similar dendritic structures on a Au seed and attributed the growth to the dose history of the experiment, that is, the local depletion of the precursors ($AuCl_3^-$ ions) by the initial electron dose led to unavailability of Au atoms. Consequently, a diffusion limited growth resulted in the dendritic morphology. However, in the experiment performed here, the depletion of the precursor was negligible due to the continuous injection of fresh solution. Instead, the flow might take away hydrolysis radicals and Au atoms, causing the lack of building elements to form particles. Indeed, it can be observed that the particles were dissolved after stopping the electron irradiation for a few minutes, as shown in Figure 5c, indicating that Au atoms were etched away from the NPs by the fresh solution. Both the dendritic shell and the faceted particle core could be dissolved with the possibility to rebuild the nanostructure by the electron irradiation again. This could allow study of the reversible formation and dissolution of NPs by simply switching on and off the electron beam while maintaining the flow in the cell. In addition, it happened occasionally that no nucleation and growth of particles was triggered in the flow mode in spite of prolonged irradiation, which was presumably due to the flowing effect that rapidly removed the hydrolysis radicals, in particular the hydrated electrons, and Au atoms within the scanned area. This warrants further investigations into the flow conditions to answer questions such as what is the effect of the flow rate on the solution chemistry, the radiolysis process, and the NP growth kinetics.

In summary, a simple and controllable way to tune complex nanoparticle growth by the electron dose rate was demonstrated here. Moreover, the process can further be expanded to other material systems, enabling studies of nucleation and growth of heterostructures containing multiple components. Besides providing insights into the interaction of electron beam with the solution in LC-TEM and the subsequent effect on the growth mechanisms of the Au NPs, this work also indicated a facile method to tune their morphology by simply changing the electron dose rates, in a similar way to an ex situ experiment using reducing agents. Different morphologies of Au NPs possess unique physical properties that can be beneficial for a wide range of applications. For instance, the 3D irregularly shaped particles with spikes produced in the 20 mM solution are similar to the ex situ synthesized Au nano-urchins that have already found applications in enhanced surface plasmon resonance.[23,24] Furthermore, a core−shell Au nanostructure can be engineered in the 1 mM solution by simply tuning the electron dose rates. The core−shell is not defined in a conventional sense in terms of chemical difference but rather in the form of different morphologies. Being a faceted particle, the core has a denser structure and is most likely crystalline, while the dendritic shell is more porous with a larger surface area and might be crystalline or amorphous. The formation is controlled by the growth mechanism which is closely dependent on the dose rate. The nanostructure can be useful for applications such as catalysis, especially when utilizing different elements for the core and the shell.[25] For a controlled growth of these NPs, LC-TEM plays an irreplaceable role.

4. CONCLUSIONS

Using LC-TEM, the effect of the electron dose rate, solute concentration, experiment conditions including the operation mode (TEM vs STEM), and the liquid cell setup (static or flow mode) on the growth mechanism and the ultimate morphology of Au NPs was systematically studied in $HAuCl_4$ aqueous solutions, providing a global picture to illustrate the complexity of the technique even when studying a simple solution. The following insights were obtained:

- The dose rate dramatically affects the growth mechanism. In general a low dose rate results in a reaction limited growth, which creates 2D plates or 3D faceted particles, while a high dose rate results in a diffusion limited growth, which creates dendritic morphology. This is in agreement with previous works.
- The dose rate threshold that defines the growth mechanism depends on the solute concentration. The threshold for the reaction-limited growth increases as the solute concentration is higher.
- To a lesser extent the growth mechanism is influenced by the imaging mode with similar morphology observed under similar conditions (dose rate and solute concentration) both in TEM and STEM.
- The liquid-cell setup, i.e., static or flow, has a significant effect on the growth of Au NPs. Particularly the flow setup continuously injects a pristine solution during the TEM investigation, constantly affects the local chemistry, and hence modifies the growth kinetics.

These insights enable the possibility to tailor novel nanostructures in situ. As a proof-of-concept, the growth of a novel Au nanostructure consisting of a faceted particle core and a dendritic shell by simply tuning the electron dose rate has been demonstrated. Therefore, the study paves the way to create complex nanostructures and gain control over their growth mechanisms in LC-TEM.

DOI: 10.1021/acs.chemmater.7b04421
Chem. Mater. 2017, 29, 10518−10525

■ ASSOCIATED CONTENT

Supporting Information

The Supporting Information is available free of charge on the ACS Publications website at DOI: 10.1021/acs.chemmater.7b04421.

Analysis of the Au NP growth in a 1 mM $HAuCl_4$ solution induced by the electron beam at a dose rate of 11.60 $e^-/(Å^2\ s)$; intensity line profiles for Au particles grown in the 5 mM and 20 mM solutions; Au NP growth in a 1 mM $HAuCl_4$ solution in the TEM mode with an intermediate dose rate of 7.60 $e^-/(Å^2\ s)$; 3D visualization of the engineered core−shell Au nanostructure (PDF)

Video 1_a (AVI)
Video 1_b (AVI)
Video 2_a (AVI)
Video 2_b (AVI)
Video 3 (AVI)
Video 4 (AVI)
Video 5 (AVI)
Video 6 (AVI)

■ AUTHOR INFORMATION

Corresponding Authors

*(Y.Z.) E-mail: yucheng.zhang@empa.ch.
*(R.E.) E-mail: rolf.erni@empa.ch.

ORCID

Yucheng Zhang: 0000-0003-3733-5851

Notes

The authors declare no competing financial interest.

■ ACKNOWLEDGMENTS

This project has received funding from the European Research Council (ERC) under EU's Horizon 2020 research and innovation program (Grant Agreement No. 681312).

■ REFERENCES

(1) de Jonge, N.; Ross, F. M. Electron microscopy of specimens in liquid. *Nat. Nanotechnol.* **2011**, *6*, 695−704.
(2) Ross, F. M. Opportunities and challenges in liquid cell electron microscopy. *Science* **2015**, *350*, aaa9886.
(3) Zheng, H. M.; Smith, R. K.; Jun, Y. W.; Kisielowski, C.; Dahmen, U.; Alivisatos, A. P. Observation of Single Colloidal Platinum Nanocrystal Growth Trajectories. *Science* **2009**, *324*, 1309−1312.
(4) Liao, H. G.; Niu, K. Y.; Zheng, H. M. Observation of growth of metal nanoparticles. *Chem. Commun.* **2013**, *49*, 11720−11727.
(5) Liao, H. G.; Zherebetskyy, D.; Xin, H. L.; Czarnik, C.; Ercius, P.; Elmlund, H.; Pan, M.; Wang, L. W.; Zheng, H. M. Facet development during platinum nanocube growth. *Science* **2014**, *345*, 916−919.
(6) Sutter, E.; Sutter, P.; Tkachenko, A. V.; Krahne, R.; de Graaf, J.; Arciniegas, M.; Manna, L. In situ microscopy of the self-assembly of branched nanocrystals in solution. *Nat. Commun.* **2016**, *7*, 11213.
(7) Park, J.; Zheng, H. M.; Lee, W. C.; Geissler, P. L.; Rabani, E.; Alivisatos, A. P. Direct Observation of Nanoparticle Superlattice Formation by Using Liquid Cell Transmission Electron Microscopy. *ACS Nano* **2012**, *6*, 2078−2085.
(8) Mehdi, B. L.; Gu, M.; Parent, L. R.; Xu, W.; Nasybulin, E. N.; Chen, X. L.; Unocic, R. R.; Xu, P. H.; Welch, D. A.; Abellan, P.; Zhang, J. G.; Liu, J.; Wang, C. M.; Arslan, I.; Evans, J.; Browning, N. D. In-Situ Electrochemical Transmission Electron Microscopy for Battery Research. *Microsc. Microanal.* **2014**, *20*, 484−492.
(9) Wu, F.; Yao, N. Advances in sealed liquid cells for in-situ TEM electrochemial investigation of lithium-ion battery. *Nano Energy* **2015**, *11*, 196−210.
(10) de Jonge, N.; Peckys, D. B.; Kremers, G. J.; Piston, D. W. Electron microscopy of whole cells in liquid with nanometer resolution. *Proc. Natl. Acad. Sci. U. S. A.* **2009**, *106*, 2159−2164.
(11) Peckys, D. B.; de Jonge, N. Liquid Scanning Transmission Electron Microscopy: Imaging Protein Complexes in their Native Environment in Whole Eukaryotic Cells. *Microsc. Microanal.* **2014**, *20*, 346−365.
(12) Nielsen, M. H.; Aloni, S.; De Yoreo, J. J. In situ TEM imaging of CaCO3 nucleation reveals coexistence of direct and indirect pathways. *Science* **2014**, *345*, 1158−1162.
(13) Schneider, N. M.; Norton, M. M.; Mendel, B. J.; Grogan, J. M.; Ross, F. M.; Bau, H. H. Electron-Water Interactions and Implications for Liquid Cell Electron Microscopy. *J. Phys. Chem. C* **2014**, *118*, 22373−22382.
(14) Abellan, P.; Woehl, T. J.; Parent, L. R.; Browning, N. D.; Evans, J. E.; Arslan, I. Factors influencing quantitative liquid (scanning) transmission electron microscopy. *Chem. Commun.* **2014**, *50*, 4873−4880.
(15) Woehl, T. J.; Abellan, P. Defining the radiation chemistry during liquid cell electron microscopy to enable visualization of nanomaterial growth and degradation dynamics. *J. Microsc.* **2017**, *265*, 135−147.
(16) Alloyeau, D.; Dachraoui, W.; Javed, Y.; Belkahla, H.; Wang, G.; Lecoq, H.; Ammar, S.; Ersen, O.; Wisnet, A.; Gazeau, F.; Ricolleau, C. Unravelling Kinetic and Thermodynamic Effects on the Growth of Gold Nanoplates by Liquid Transmission Electron Microscopy. *Nano Lett.* **2015**, *15*, 2574−2581.
(17) Lifshitz, I. M.; Slyozov, V. V. THE KINETICS OF PRECIPITATION FROM SUPERSATURATED SOLID SOLUTIONS. *J. Phys. Chem. Solids* **1961**, *19*, 35−50.
(18) Viswanatha, R.; Sarma, D. D., Growth of Nanocrystals in Solution. In *Nanomaterials Chemistry*; Wiley-VCH Verlag GmbH & Co. KGaA: 2007; pp 139−170.
(19) Woehl, T. J.; Evans, J. E.; Arslan, L.; Ristenpart, W. D.; Browning, N. D. Direct in Situ Determination of the Mechanisms Controlling Nanoparticle Nucleation and Growth. *ACS Nano* **2012**, *6*, 8599−8610.
(20) Ahmad, N.; Le Bouar, Y.; Ricolleau, C.; Alloyeau, D. Growth of dendritic nanostructures by liquid-cell transmission electron microscopy: a reflection of the electron-irradiation history. *Adv. Struct. Chem. Imaging* **2017**, *2*, 9.
(21) Kraus, T.; de Jonge, N. Dendritic Gold Nanowire Growth Observed in Liquid with Transmission Electron Microscopy. *Langmuir* **2013**, *29*, 8427−8432.
(22) Hermannsdörfer, J.; de Jonge, N.; Verch, A. Electron beam induced chemistry of gold nanoparticles in saline solution. *Chem. Commun.* **2015**, *51*, 16393−16396.
(23) Bakr, O. M.; Wunsch, B. H.; Stellacci, F. High-yield synthesis of multi-branched urchin-like gold nanoparticles. *Chem. Mater.* **2006**, *18*, 3297−3301.
(24) Vijayaraghavan, P.; Liu, C. H.; Hwang, K. C. Synthesis of Multibranched Gold Nanoechinus Using a Gemini Cationic Surfactant and Its Application for Surface Enhanced Raman Scattering. *ACS Appl. Mater. Interfaces* **2016**, *8*, 23909−23919.
(25) Huang, J. F.; Vongehr, S.; Tang, S. C.; Lu, H. M.; Shen, J. C.; Meng, X. K. Ag Dendrite-Based Au/Ag Bimetallic Nanostructures with Strongly Enhanced Catalytic Activity. *Langmuir* **2009**, *25*, 11890−11896.

DOI: 10.1021/acs.chemmater.7b04421
Chem. Mater. 2017, 29, 10518−10525